Supporting Information

Micro-structuring to improve the thermal stability of GeSn layers

Valentina Bonino[1], Nicolas Pauc[2], Vincent Calvo[2], Marvin Frauenrath[3], Jean-Michel Hartmann[3], Alexei Chelnokov[3], Vincent Reboud[3], Martin Rosenthal[1], Jaime Segura-Ruiz[1,*]

[1] ESRF – The European Synchrotron, 71 Avenue des Martyrs, 38000 Grenoble, France

[2] Univ. Grenoble Alpes, CEA, Grenoble INP, IRIG, PHELIQS, 38000 Grenoble, France

[3] University of Grenoble Alpes, CEA, LETI, F-38054 Grenoble, France

* jaime.segura@esrf.fr

Figure S1: Micro-structuring of the $Ge_{1-x}Sn_x$ layer.

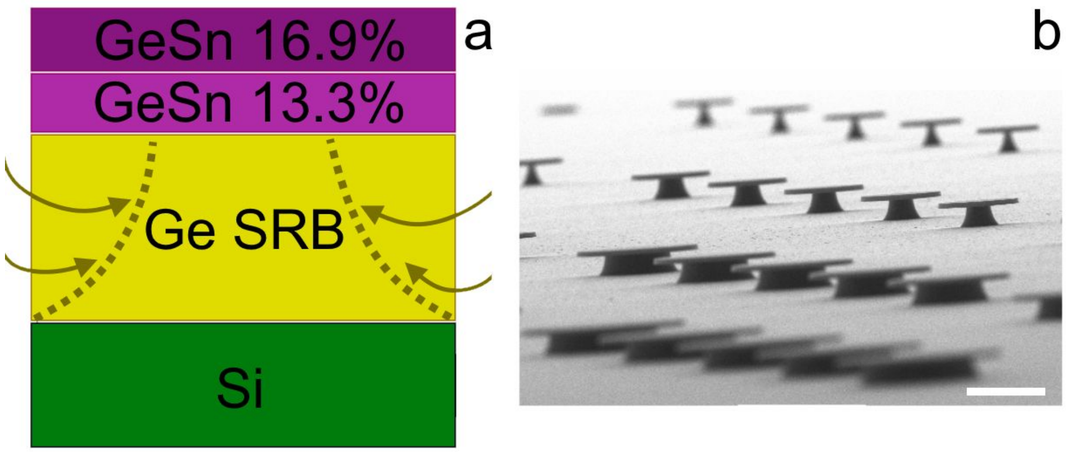

a. Schematic representation of the structure of a P08 blanket layer. The arrows and the dashed lines indicate the parts that were removed during the etching process to obtain micro-disks. b. SEM view of an array of micro-disks. Scale bar, 10 µm.

Figure S2: X-ray beam size and XRF spectrum fitting.

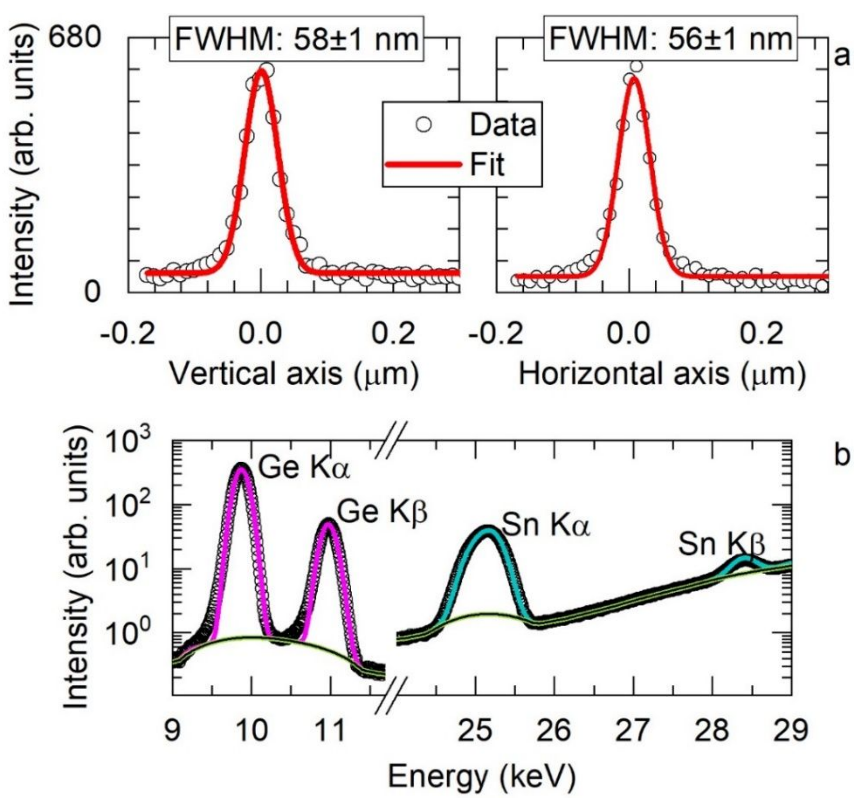

a, Vertical and horizontal X-ray nanobeam profiles. b, Typical XRF spectrum measured from a $Ge_{1-x}Sn_x$ micro-disk showing the Ge K and Sn K XRF lines (open symbols). Solid lines indicate the best fit obtained via PYMCA of the XRF peaks and background.

Figure S3: Profiles of the Sn distribution around the segregation front in a $Ge_{1-x}Sn_x$ blanket layer (left) and a micro-disk (right).

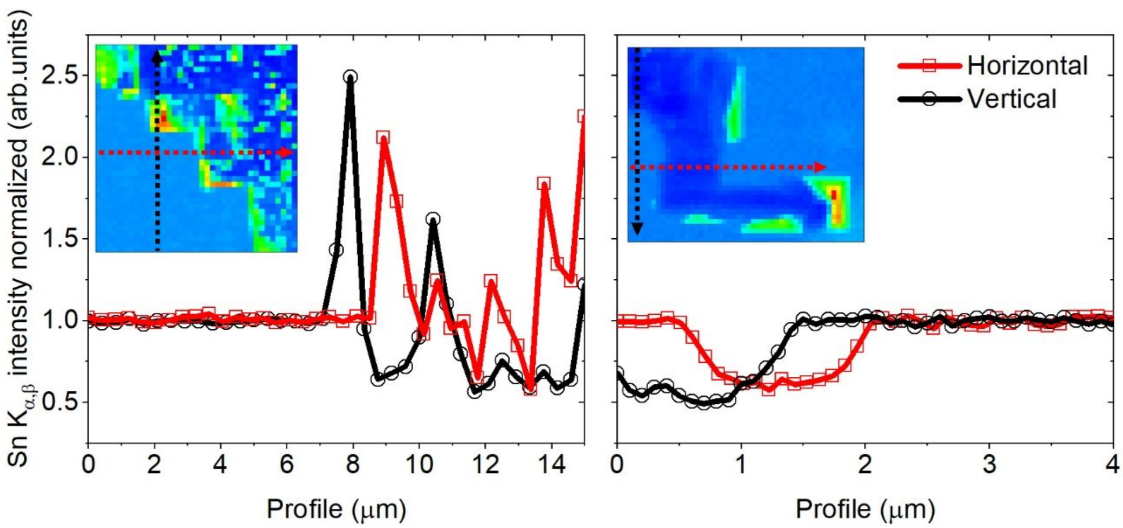

Horizontal and vertical profiles of the Sn distribution in P07 blanket $Ge_{1-x}Sn_x$ layer (bottom to top and left to right) and a P07 micro-disk (20 µm diameter) after 20 minutes of annealing at 350°C and 400°C, respectively.

The results shown in Fig. S3 suggest that there was no Sn segregation in the surface nor in the bulk of the blanket layer (micro-disk) beyond the segregation front (path). The high penetration of the 33 keV X-rays used (around 170 μm in Ge) enabled to probe the entire $Ge_{1-x}Sn_x$ layer thickness. Despite the high spatial resolution and sensitivity of the XRF technique, this result cannot completely discard the existence of small segregates (few nanometers) out of the segregated region that could not be detected.

Figure S4: Elemental distribution in annealed pseudomorphic $Ge_{1-x}Sn_x$ layers and $Ge_{1-x}Sn_x$ micro-disks.

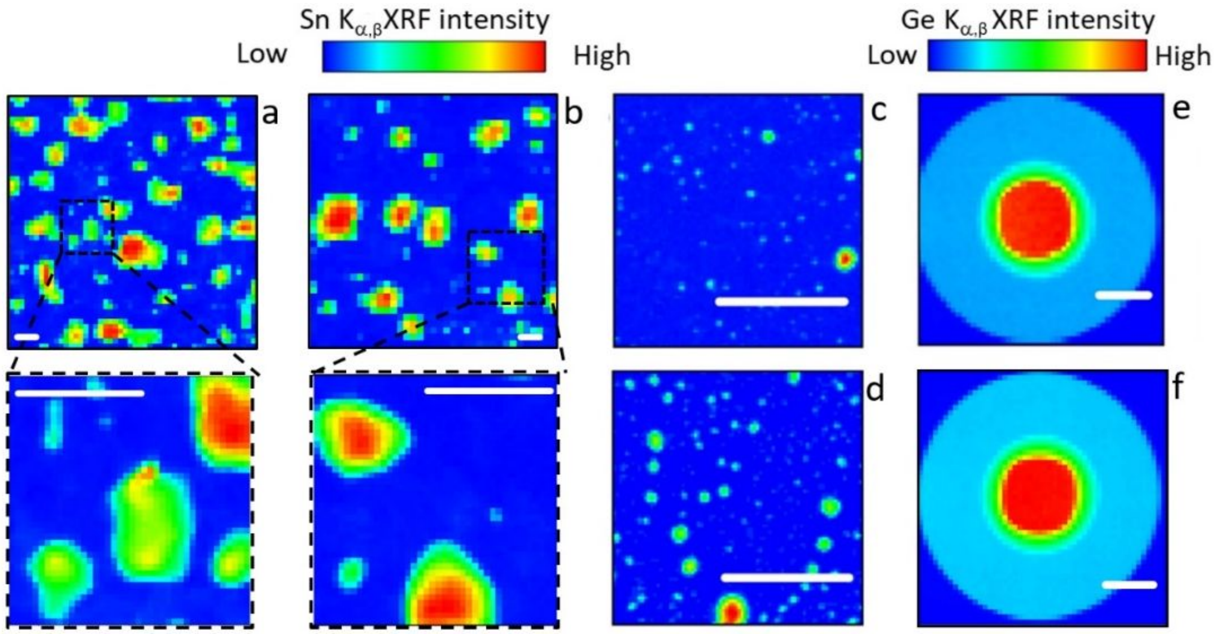

a, b. Sn distribution in $Ge_{1-x}Sn_x$ layers P08 (a) and P07 (b), with 16.9% and 12.7% of Sn on top, segregated after 20 minutes of annealing at 350°C. c, d. Sn distribution in $Ge_{1-x}Sn_x$ pseudomorphic layers with Sn concentrations - thicknesses of 12.5% - 29.5 nm (c) and 14.9% - 31 nm (d), grown at 313°C and 301°C, respectively, segregated after 20 minutes of annealing at 350°C. e,f. Ge distribution in P08 and P07 non-segregated micro-disks shown in Fig. 1e,f., respectively, after 20 minutes of annealing at 350°C. Scale bars, 2 µm.

The comparison between the Sn-distribution in thick layers P07 and P08 (a,b) and that of pseudomorphic layers (c,d) with similar Sn concentrations, suggests that there is a different mechanism for the propagation of Sn segregates in these two types of layers. In the first case, the propagation is dominated by the <110> crystallographic orientation, whereas for the pseudomorphic layers the random distribution of segregates suggests a free-propagation. Furthermore, pseudomorphic layers showed small rounded segregates, different from the large geometric ones observed in thick layers. These differences may be due to the high compressive strain in pseudomorphic layers. Meanwhile, the thick, partially relaxed GeSn layers P07 and P08 had significant surface cross-hatches, i.e. regular arrays of <110> undulations on the surfaces stemming from the presence of periodic strain fields underneath, that might have guided the glide of Sn segregates. However, we cannot exclude that the reduced thickness of the pseudomorphic layers, with therefore a lower Sn reservoir, could also have had an impact on the size and distribution of metal segregates. Fig. S4e,f. show the complementary Ge distribution of the Sn-distribution maps shown in Fig. 1e,f. The high Ge intensity in the central area comes from the Ge pedestal.

Figure S5: Sn distribution in micro-disks annealed at 350°C during 1 and 2 hours.

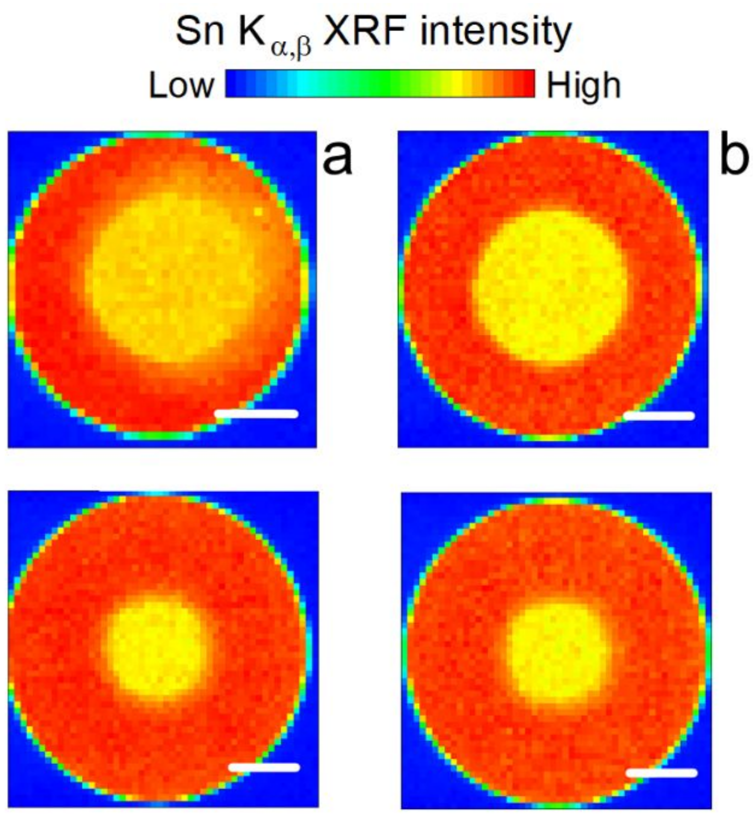

a,b. Sn-K distribution maps in non-segregated micro-disks P08 (a) and P07 (b) 10 µm in diameter after annealing at 350°C during 1 hour (top) and 2 hours (bottom). Scale bars, 2 µm.

Sn distribution maps of annealed micro-disks P07 and P08 indicates that, even for the higher Sn-concentration, there is no Sn-segregation at 350°C even after a long thermal annealing of 2 hours.

Figure S6: Micro-Raman spectra associated with low Sn content areas after segregation in micro-disks.

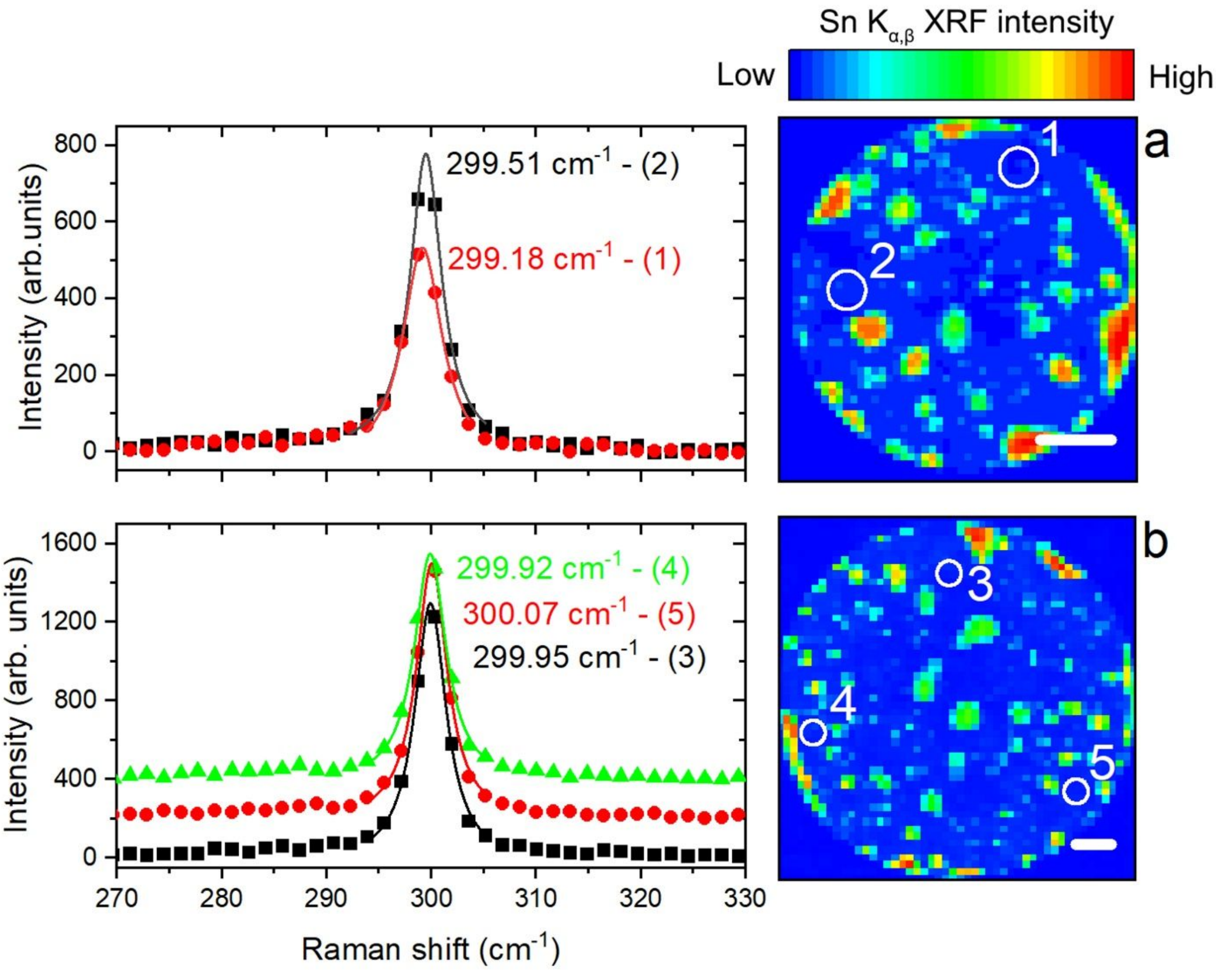

a,b. Micro-Raman spectra collected in the areas circled in the corresponding XRF Sn-distribution maps for the micro-disks P08 (a) and P07 (b) annealed at 400°C during 20 minutes. Scale bars, 2 µm.

The micro-Raman spectra measured in the points shown in the XRF Sn-distribution maps show the Ge-Ge phonon mode and its value. The frequencies of the Ge-Ge phonon mode shown for each spectrum were obtained from a fitting using a Lorentzian function. They are given in Table S1.

Figure S7: Reciprocal space maps of blanket layers P07 and P08around the (224) X-ray diffraction order.

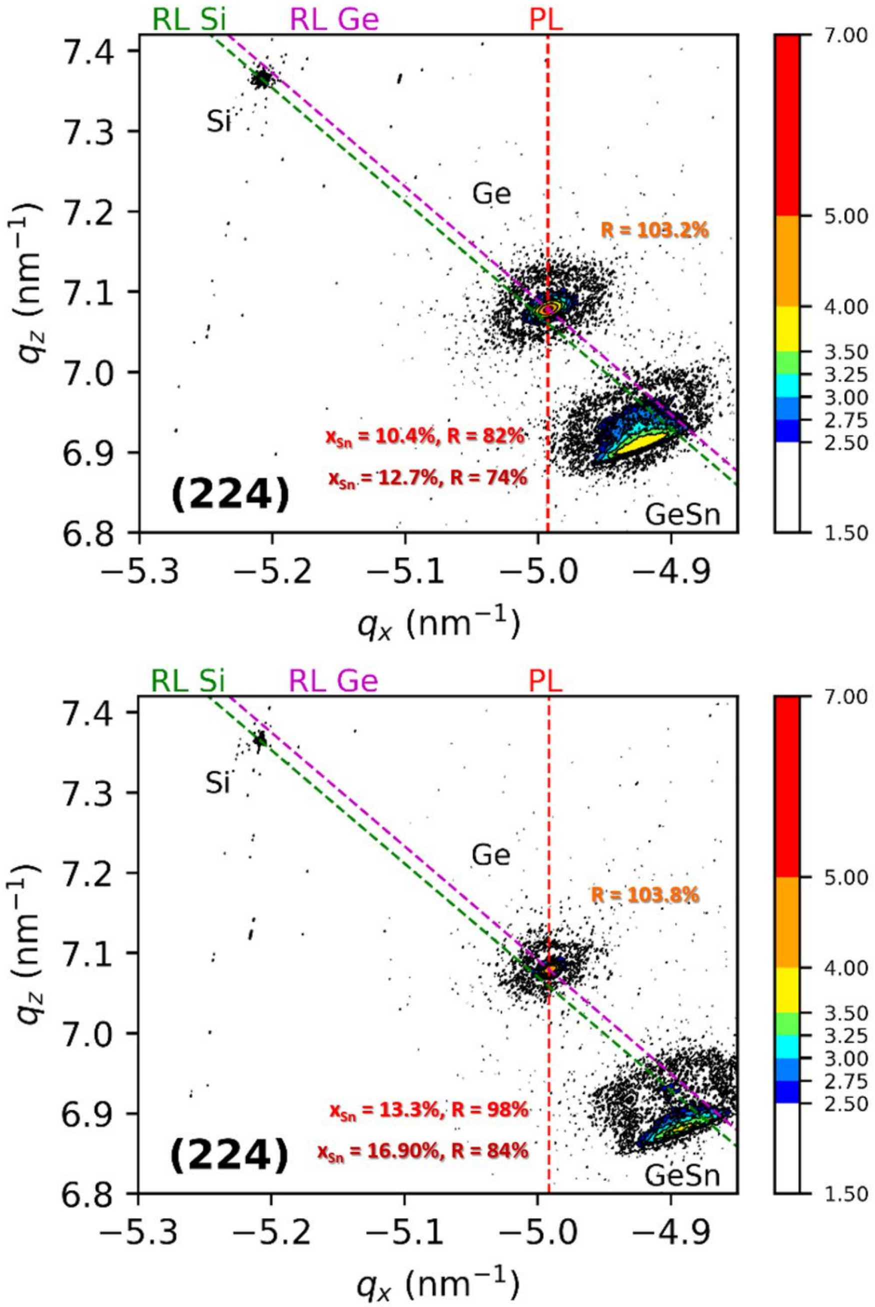

Reciprocal Space Maps around the (224) X-ray diffraction order for layers P07 (left) and P08 (right). Relaxation degree and Sn concentrations are indicated for each sample and sub-layer.

Table S1. Sn atomic concentration in non-annealed micro-disks, and in segregated and non-segregated micro-disks after annealing at 400°C during 20 minutes. Sn concentrations were calculated from the frequency of the Ge-Ge mode and from the fitting of the XRF spectra for each sample (Fig S6).

Micro-disk		Ge-Ge peak position (cm $^{-1}$)	Average Sn % - Raman (at. %)	Average Sn % - XRF (at. %)
P08 – non-annealed		287.0	15.8	13.4
P07 – non-annealed		289.6	12.8	10.8
P08 – annealed non-segregated:		287.3	15.5	13.3
P07 – annealed non-segregated		290.6	11.7	10.6
P08 – annealed segregated	1.	299.2	1.9	2.8
	2.	299.5	1.6	3.0
P07 – annealed segregated	3.	299.9	1.1	3.6
	4.	300.1	0.9	3.2
	5.	300.0	1.0	3.1

The micro-structured layer P08, with the highest nominal Sn concentration (around 17%), appears to be the most Sn-depleted one (Fig. 3c). This suggests that the higher the Sn content in the layer is, the higher the Sn depletion after segregation will be.

The maximum error on the average Sn% content obtained from XRF for non-annealed and non-segregated samples is of 0.2%. This error was calculated considering confidence of 2 times the standard deviation (95%). It is mainly limited by the accumulation time per pixel used for the XRF mapping. Raman spectral resolution is of 0.5 cm^{-1}. This results in an error on the Sn content around 1%.

There is a good agreement between Raman and XRF estimated concentrations for segregated micro-disks, and a small disagreement in the case of non-annealed and non-segregated ones. The latter is likely due to the different regions probed by micro-Raman (near-surface) and XRF (full thickness). This would indicate that Sn concentration in segregated micro-disks is homogeneous in depth, whereas the step graded composition profile of non-segregated annealed micro-disks is preserved.

Table S2. Integrated intensity of the micro-PL spectra of several 8 μm diameter micro-disks fabricated from sample P08 (16.9% of Sn) measured at 20K.

Sample	**PL integrated signal (μV)**	**Average PL integrated signal (μV)**	**Gain**
Etched, non-annealed	56, 67, 70	64	
Annealed at 350°C, 20min	290, 300, 322	304	4.7
Annealed at 350°C, 2h	490, 420, 420, 405, 450	437	6.8
Annealed at 400°C, 20min	490, 430, 410, 450	445	7.0

The values shown for each sample correspond to the integrated intensity of the complete PL emission (including whispering gallery modes). Several measurements were performed for each sample and the gain compared with the integrated intensity of the non-annealed disks was calculated using the average of the several measurements.